

# How Well Do the CMIP5 Models Simulate the Antarctic Atmospheric Energy Budget?

MICHAEL PREVIDI AND KAREN L. SMITH

*Lamont–Doherty Earth Observatory of Columbia University, Palisades, New York*

LORENZO M. POLVANI

*Lamont–Doherty Earth Observatory of Columbia University, Palisades, and Department of Applied Physics and Applied Mathematics, and Department of Earth and Environmental Sciences, Columbia University, New York, New York*

(Manuscript received 6 January 2015, in final form 5 June 2015)

## ABSTRACT

The authors evaluate 23 coupled atmosphere–ocean general circulation models from phase 5 of CMIP (CMIP5) in terms of their ability to simulate the observed climatological mean energy budget of the Antarctic atmosphere. While the models are shown to capture the gross features of the energy budget well [e.g., the observed two-way balance between the top-of-atmosphere (TOA) net radiation and horizontal convergence of atmospheric energy transport], the simulated TOA absorbed shortwave (SW) radiation is too large during austral summer. In the multimodel mean, this excessive absorption reaches approximately  $10 \text{ W m}^{-2}$ , with even larger biases (up to  $25\text{--}30 \text{ W m}^{-2}$ ) in individual models. Previous studies have identified similar climate model biases in the TOA net SW radiation at Southern Hemisphere midlatitudes and have attributed these biases to errors in the simulated cloud cover. Over the Antarctic, though, model cloud errors are of secondary importance, and biases in the simulated TOA net SW flux are instead driven mainly by biases in the clear-sky SW reflection. The latter are likely related in part to the models' underestimation of the observed annual minimum in Antarctic sea ice extent, thus underscoring the importance of sea ice in the Antarctic energy budget. Finally, substantial differences in the climatological surface energy fluxes between existing observational datasets preclude any meaningful assessment of model skill in simulating these fluxes.

## 1. Introduction

Historically, the climate of the Southern Hemisphere has been relatively understudied in comparison to that of the Northern Hemisphere and hence remains poorly understood. This stems mainly from the paucity of Southern Hemisphere observational data, particularly over the remote Southern Ocean and Antarctic continent. The situation has changed dramatically during the past few decades, however, as global-scale observations (e.g., satellite data and Argo oceanographic profiles) have provided new insights into the workings of the Southern Hemisphere climate system.

Among other things, our enhanced observational capacity has led to an increased focus in recent years on climate model performance in the Southern Hemisphere.

Through a number of studies, it has become apparent that current models are deficient in their simulation of several key aspects of Southern Hemisphere climate. For example, [Trenberth and Fasullo \(2010\)](#) noted that the atmosphere–ocean general circulation models (GCMs) from phase 3 of the Coupled Model Intercomparison Project (CMIP3) simulate excessive absorption of solar radiation at Southern Hemisphere middle and high latitudes—a problem that they attributed to errors in the models' cloud field. These same models also simulate too little solar radiation absorption in the Southern Hemisphere tropics (again related to clouds), implying an unrealistically weak poleward energy transport by the atmosphere and ocean. In accordance with this, [Chang et al. \(2013\)](#) concluded that the CMIP3 models simulate storm-track activity that is generally too weak in the Southern Hemisphere compared to observations. The CMIP3 model biases described here are also present in the more recent generation of CMIP5 coupled GCMs (e.g., [Ceppi et al. 2012](#); [Chang et al. 2012](#)).

---

*Corresponding author address:* Dr. Michael Previdi, Lamont–Doherty Earth Observatory of Columbia University, 61 Route 9W, Palisades, NY 10964.  
E-mail: mprevidi@ldeo.columbia.edu

Another well-known climate model bias in the Southern Hemisphere, in both the CMIP3 and CMIP5 models, is in the mean position of the midlatitude eddy-driven jet, with most models tending to place the jet too far equatorward (e.g., [Kidston and Gerber 2010](#); [Barnes and Hartmann 2010](#); [Bracegirdle et al. 2013](#)). Although the causes of this bias are not completely understood, it may be linked, at least in part, to the biases in solar radiation absorption at Southern Hemisphere midlatitudes discussed above ([Ceppi et al. 2012](#); see also [Grise and Polvani 2014](#)). The latter biases have also been linked to the so-called “double intertropical convergence zone” problem in climate models, in which excessive precipitation is simulated in the Southern Hemisphere tropics ([Hwang and Frierson 2013](#); [Li and Xie 2014](#)).

Closer to the Antarctic continent, additional studies have further assessed the credibility of model simulations of the atmospheric circulation, as well as the seasonal cycle of Antarctic sea ice extent (SIE). [Hosking et al. \(2013\)](#) examined the representation of the Amundsen–Bellingshausen Seas low and its seasonal variability in the CMIP5 models. They concluded that most models exhibit definite biases, particularly in terms of the longitudinal position of the low, with implications for the ability to realistically simulate the climate of West Antarctica. [Turner et al. \(2013\)](#) focused on Antarctic SIE in CMIP5 and found that the majority of models simulate an annual SIE minimum that is too small compared to observations. Additionally, several models were shown to underestimate the observed seasonal maximum in SIE. These model biases in the seasonal cycle of Antarctic sea ice can have strong impacts on the simulated deep convection in the Southern Ocean ([Heuzé et al. 2013](#)).

[Turner et al. \(2013\)](#) also noted differences between modeled and observed SIE trends over the late twentieth and early twenty-first centuries. While the observed trend based on satellite measurements is positive during every month of the year, the majority of models were found to simulate a diminishing ice cover. It is important to point out, however, that the cause of this model–data mismatch is still a matter of debate (e.g., [Polvani and Smith 2013](#); [Bintanja et al. 2013](#); [Fan et al. 2014](#); [Gagné et al. 2015](#)), and it is not clear that the mismatch necessarily reflects an error in the models (e.g., an unrealistic response to climate forcing).

Finally, although the discussion thus far has focused primarily on the climatological mean state in the Southern Hemisphere, additional investigations have further evaluated climate model skill in simulating certain aspects of interannual variability. For instance, in a recent paper, [Grise and Polvani \(2014\)](#) examined cloud

changes and cloud-radiative anomalies associated with interannual variations in the latitude of the Southern Hemisphere westerly jet. They determined that the simulated cloud response to jet shifts differs markedly from observations in a substantial fraction of CMIP5 models. In these models, poleward shifts of the jet are accompanied by reductions in total cloud fraction at Southern Hemisphere midlatitudes, which contribute to enhanced shortwave radiative warming there. This has implications for model projections of future warming, as the jet is also simulated to move poleward in response to increasing concentrations of atmospheric CO<sub>2</sub>. In an analogous manner, some of the other model biases in simulating the present-day climate discussed above have also been linked to future projections. Notably, models with the largest equatorward biases in present-day jet latitude tend to simulate the largest poleward shifts of the jet during the twenty-first century ([Kidston and Gerber 2010](#)).

In this paper, we add to the growing body of work assessing climate model performance in the Southern Hemisphere by evaluating how well the CMIP5 coupled GCMs simulate the climatological mean Antarctic atmospheric energy budget. Model output will be compared with a recently published observational estimate of the Antarctic energy budget ([Previdi et al. 2013](#), hereinafter [PSP13](#)) for the period 2001–10. Where possible, results will be interpreted within the context of earlier work discussed in this section.

## 2. Data and methods

### a. Energy budget formulation

We will define the Antarctic atmospheric energy budget as in [PSP13](#). A full derivation of the energy budget is provided by [Smith et al. \(2013\)](#). Here, we will describe its primary elements.

The energy budget of an atmospheric column extending from the surface (SFC) to the top of the atmosphere (TOA) can be written as

$$\frac{\partial E}{\partial t} = F_{\text{TOA:NET}} + F_{\text{SFC:NET}} + F_{\text{WALL}}, \quad (1)$$

where  $\partial E/\partial t$  is the storage of energy within the column,  $F_{\text{TOA:NET}}$  is the TOA net radiative energy flux,  $F_{\text{SFC:NET}}$  is the SFC net energy flux, and  $F_{\text{WALL}}$  is the vertically integrated horizontal convergence of atmospheric energy transport. We can expand the energy storage term as

$$\frac{\partial E}{\partial t} = \frac{\partial}{\partial t} \frac{1}{g} \int_0^{p_{\text{SFC}}} (c_p T + k + Lq + \Phi_{\text{SFC}}) dp, \quad (2)$$

where  $g$  is the acceleration due to gravity,  $p$  is the pressure,  $p_{\text{SFC}}$  is the surface pressure,  $c_p$  is the specific heat of air at constant pressure,  $T$  is absolute temperature,  $k$  is the kinetic energy,  $L$  is the latent heat of vaporization,  $q$  is the specific humidity, and  $\Phi_{\text{SFC}}$  is the surface geopotential. Similarly, expanding the terms on the right-hand side of Eq. (1), we obtain

$$F_{\text{TOA:NET}} = F_{\text{TOA:SW}} + F_{\text{TOA:LW}}, \quad (3)$$

$$F_{\text{SFC:NET}} = F_{\text{SFC:SW}} + F_{\text{SFC:LW}} + F_{\text{SFC:LH+SH}}, \quad \text{and} \quad (4)$$

$$F_{\text{WALL}} = -\nabla \cdot \frac{1}{g} \int_0^{p_{\text{SFC}}} (c_p T + k + Lq + \Phi) \mathbf{v} dp. \quad (5)$$

One notes that the net TOA radiative flux  $F_{\text{TOA:NET}}$  comprises net shortwave (SW) and longwave (LW) components [Eq. (3)]. The net SFC energy flux [Eq. (4)] also includes SW and LW radiative fluxes and additionally the nonradiative fluxes of latent heat (LH) and sensible heat (SH). Finally, Eq. (5) states that the total atmospheric energy flux convergence  $F_{\text{WALL}}$  is the sum of the convergence of the internal, kinetic, latent, and potential energy fluxes, with  $\mathbf{v}$  the horizontal wind vector.

Following PSP13, all energy budget terms will be area averaged over the region  $70^\circ\text{--}90^\circ\text{S}$  (see Fig. 1). Terms are defined to be positive when they contribute to a gain of energy for the atmospheric column. Thus, downward fluxes at the TOA, upward fluxes at the SFC, and horizontal energy flux convergence are all positive.

### b. Observational and CMIP5 data

As noted above, the observed Antarctic atmospheric energy budget that will form the basis for our CMIP5 evaluation is the one described by PSP13. That study used Clouds and the Earth's Radiant Energy System (CERES) TOA radiative fluxes from the Energy Balanced and Filled (EBAF TOA) dataset (Loeb et al. 2009), while surface energy fluxes and atmospheric energy storage ( $\partial E/\partial t$ ) were based on ERA-Interim (Dee et al. 2011). Lastly, the horizontal convergence of atmospheric energy transport ( $F_{\text{WALL}}$ ) was computed in two ways: as the energy budget residual and directly using ERA-Interim vertically integrated and mass-adjusted (Trenberth 1991) northward energy fluxes. These two methods of computing  $F_{\text{WALL}}$  were found to yield very similar results (see Fig. 2 in PSP13).

For the current work, we will use the observed values of the surface energy fluxes and atmospheric energy storage that were presented in PSP13 (see their Table 1). Additionally, we will compare the CMIP5 simulated surface energy fluxes with two other observational products: the CERES EBAF surface dataset (Kato et al. 2013) and the NCEP–NCAR reanalysis (Kalnay et al.

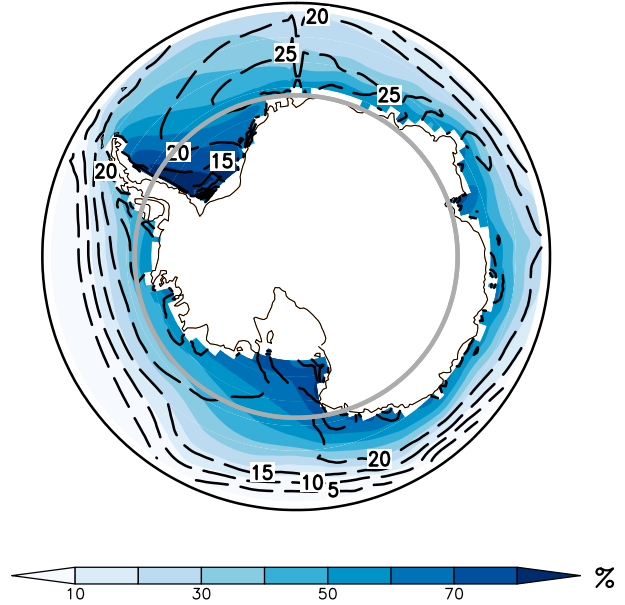


FIG. 1. Antarctica and the Southern Ocean. The present study focuses on the atmospheric energy budget over  $70^\circ\text{--}90^\circ\text{S}$ , which is the area enclosed within the gray circle. In this region, the CMIP5 multimodel and annual-mean sea ice concentration (SIC; shading) is at a maximum. There is also a significant amount of variability in SIC between models, as indicated by the SIC intermodel standard deviation (dashed contours; %). As discussed in the text, this SIC variability is important for understanding differences in the simulated energy budget between models.

1996). Both of these observational products provide estimates of the surface radiative fluxes ( $F_{\text{SFC:SW}}$  and  $F_{\text{SFC:LW}}$ ), with the NCEP–NCAR reanalysis also providing the surface nonradiative flux ( $F_{\text{SFC:LH+SH}}$ ).

For the observed TOA fluxes in the present study, we update the values given by PSP13 by utilizing the latest version of the CERES EBAF TOA dataset (version 2.8, as opposed to version 2.6, which was used in PSP13; note that the CERES EBAF surface dataset used here is also version 2.8). This has a very small impact on the polar-cap-averaged TOA radiation, changing the climatological mean fluxes by at most  $1\text{--}2\text{ W m}^{-2}$  during some months. Finally, we compute observed  $F_{\text{WALL}}$  here directly from ERA-Interim data, as described above.

We compare the observed climatological mean energy budget for 2001–10 with simulations from 23 coupled atmosphere–ocean GCMs that were included in CMIP5. For each GCM, we concatenated the last 5 years of the historical simulation (2001–05) and the first 5 years of the representative concentration pathway 4.5 (RCP4.5) simulation (2006–10), using all available ensemble members from each model. The GCMs considered (with number of ensemble members in parentheses after each GCM) are as follows: ACCESS1.0 (1), BCC\_CSM1.1 (1), CanESM2 (5), CCSM4 (6), CESM1(WACCM) (3),

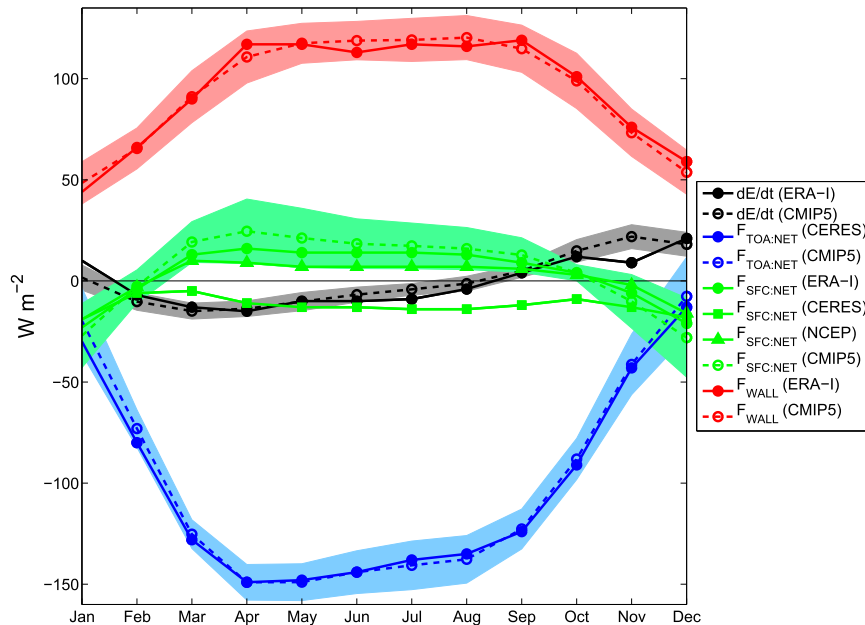


FIG. 2. The observed and CMIP5 simulated climatological mean Antarctic energy budget during 2001–2010. Energy budget terms in the legend are defined in the text. For each term, observed values are plotted using solid lines, and CMIP5 multimodel mean values are plotted using dashed lines. Shading indicates the  $2\sigma$  model spread about the mean. For  $F_{\text{SFC:NET}}$ , three different observational estimates are plotted:  $F_{\text{SFC:NET}}$  from ERA-Interim (ERA-I),  $F_{\text{SFC:NET}}$  computed as the sum of the CERES EBAF surface radiative fluxes and the ERA-Interim nonradiative (LH + SH) flux (CERES), and  $F_{\text{SFC:NET}}$  from the NCEP–NCAR reanalysis (NCEP).

CNRM-CM5 (1), FGOALS-g2 (1), GFDL CM3 (1), GFDL-ESM2G (1), GFDL-ESM2M (1), GISS-E2-R (5), HadGEM2-CC (1), HadGEM2-ES (4), IPSL-CM5A-LR (4), IPSL-CM5A-MR (1), IPSL-CM5B-LR (1), MIROC5 (5), MIROC-ESM (1), MIROC-ESM-CHEM (1), MPI-ESM-LR (3), MPI-ESM-MR (3), MRI-CGCM3 (1), and NorESM1-M (1). For models with multiple ensemble members, we use the ensemble mean in all subsequent analyses. (Expansions of the GCM acronyms are available at <http://www.ametsoc.org/PubsAcronymList>.)

Monthly mean TOA and surface energy fluxes for each GCM were downloaded directly from the CMIP5 archive. The atmospheric energy storage was calculated from Eq. (2), using model-simulated monthly profiles of temperature, specific humidity, and zonal ( $u$ ) and meridional ( $v$ ) wind components, as well as the surface geopotential (orography). The vertical profiles of these various fields were acquired on the 17 CMIP5 standard pressure levels ranging from 10 to 1000 hPa, with the time-varying surface pressure used to discard pressure levels below the surface. Finally, the  $F_{\text{WALL}}$  term in the atmospheric energy budget was computed as a residual for all GCMs. We explored the possibility of computing this term directly, as we have done for the observational

data, but obtained unrealistic values of  $F_{\text{WALL}}$  for the models examined. The residual approach was therefore adopted since it yielded much better agreement with observations.

### 3. CMIP5 simulations of the Antarctic energy budget

#### a. Overall assessment

The climatological annual cycle of the Antarctic atmospheric energy budget [i.e., the different terms in Eq. (1)] is shown in Fig. 2 for models and observations. Solid lines represent the observed values (see section 2b), dashed lines are the CMIP5 multimodel means, and shading denotes the  $2\sigma$  model spread about the mean.

To first order, it is clear that the CMIP5 models do well in simulating the climatological mean energy budget, both in terms of representing correctly the relative magnitudes of different terms and in realistically simulating the seasonal cycle of individual terms. As discussed by PSP13, the primary balance in the Antarctic energy budget is between the TOA net radiation (which is generally negative throughout the year) and the horizontal convergence of atmospheric energy transport (which is positive). Thus, the Antarctic atmosphere has a

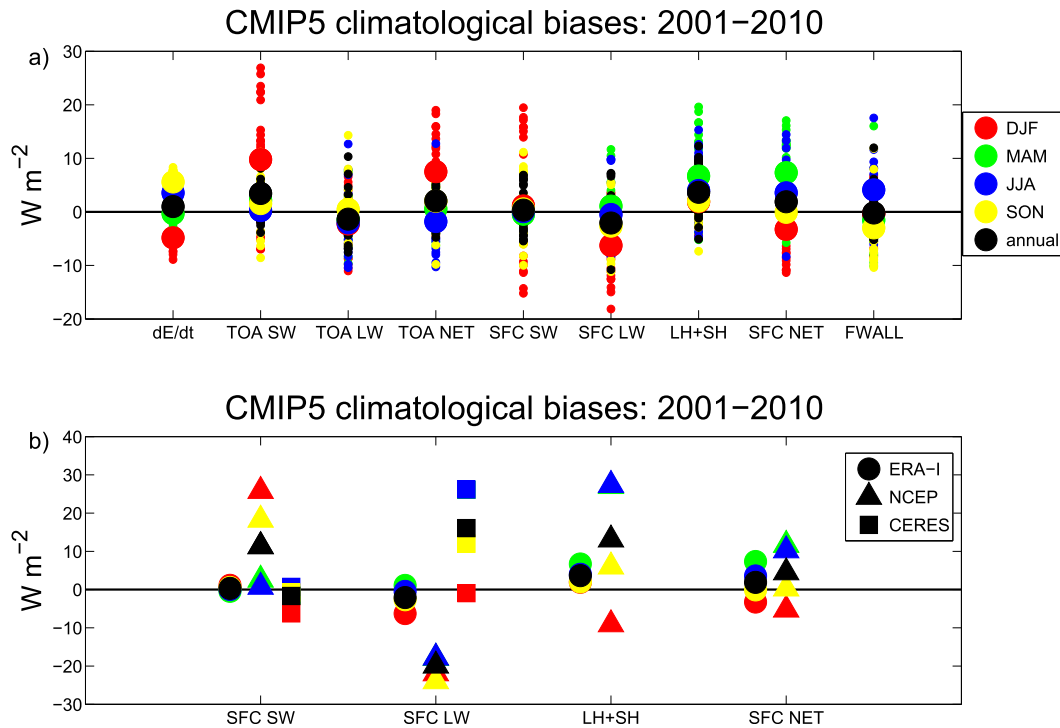


FIG. 3. (a) CMIP5 climatological mean energy budget biases. Biases in the TOA fluxes are relative to CERES EBAF TOA data, while biases in all other terms are relative to ERA-Interim. Large dots represent the multimodel mean, while small dots represent individual models. Different colors depict different seasons and the annual mean (see the legend). (b) CMIP5 multimodel mean biases in the surface energy fluxes relative to three different observational products: ERA-Interim (circles), NCEP-NCAR reanalysis (triangles), and CERES EBAF surface data (squares). Different colors for individual seasons and the annual mean are as those in (a).

net loss of radiative energy at the TOA, which tends to be compensated for by a gain of energy from atmospheric transport into the polar cap. The flux  $F_{TOA:NET}$  is at a minimum during the cold half of the year (April–September), corresponding with the annual minimum in incoming solar radiation (insolation). Accordingly, maximum values of  $F_{WALL}$  occur during this same 6-month period. The level of agreement between model-simulated and observed values of  $F_{TOA:NET}$  is generally highest during the cold half of the year and lowest during the warm half of the year (October–March). As will be shown, this is mostly due to model difficulties in realistically simulating SW radiative transfer during austral summer.

Although less pronounced than for the TOA radiation and atmospheric energy transport, the net surface energy flux (green lines in Fig. 2) and atmospheric energy storage (black lines in Fig. 2) also display discernible seasonal cycles. The clear exception to this is the net surface energy flux curve labeled “ $F_{SFC:NET}$  (CERES)” in Fig. 2, which represents the sum of the CERES EBAF surface radiative fluxes and the ERA-Interim surface nonradiative (LH + SH) flux. The flux  $F_{SFC:NET}$  (CERES) displays very little seasonal variation and is of

opposite sign to the other  $F_{SFC:NET}$  curves (both modeled and observed) during most of the year (March–October). Differences in these various estimates of the Antarctic net surface energy flux are examined in greater detail below.

In Fig. 3a, the CMIP5 climatological biases in each energy budget component are shown. The bias for a given component is defined as the simulated value minus the observed value, with observed TOA fluxes taken from the CERES EBAF TOA dataset and observed values of all other terms taken from ERA-Interim. Biases are shown for individual seasons and the annual mean as well as for individual models (small dots) and the multimodel mean (large dots). As one can see from the labels on the abscissa, we include not just the net TOA and surface fluxes (as in Fig. 2) but also the individual components of these net fluxes [i.e., the terms on the right-hand side of Eqs. (3) and (4)].

Figure 3a indicates that the largest multimodel mean bias (of about  $+10 W m^{-2}$ ) occurs for the TOA SW radiation during the December–February (DJF) season. For individual models, the bias is considerably larger (as high as  $+25$ – $30 W m^{-2}$ ). The positive multimodel mean

bias in the TOA SW flux, which indicates excessive absorption of SW radiation, is reflected in the net TOA radiation. In section 3b, we discuss the causes of this excessive SW absorption.

At the surface, there are discernible differences in the energy fluxes between the CMIP5 models and ERA-Interim (Fig. 3a). Most notable are a negative multimodel mean bias of about  $-6 \text{ W m}^{-2}$  in the surface LW flux during DJF and a positive multimodel mean bias of about  $+7 \text{ W m}^{-2}$  in the surface LH + SH flux during March–May (MAM). The latter is reflected as a similar bias in the MAM net surface energy flux. Given the clear differences in  $F_{\text{SFC:NET}}$  between different observational products (see Fig. 2), however, one can question the extent to which these inferred model biases are dependent on the choice of observational dataset used for model validation.

To answer this question, we plot in Fig. 3b the CMIP5 multimodel mean biases in the surface energy fluxes relative to the three observational products discussed above. For the DJF surface LW flux, the  $-6 \text{ W m}^{-2}$  model bias relative to ERA-Interim becomes a  $-22 \text{ W m}^{-2}$  bias relative to the NCEP–NCAR reanalysis but only a  $-1 \text{ W m}^{-2}$  bias relative to the CERES EBAF surface dataset. Similarly, the inferred multimodel mean bias in the MAM LH + SH flux depends significantly on the observational estimate that is employed, with values of  $+7$  and  $+27 \text{ W m}^{-2}$  when computed relative to ERA-Interim and the NCEP–NCAR reanalysis, respectively. For some of the other biases shown in Fig. 3b, even the sign can change depending on the observational dataset considered. It is not immediately apparent which of these three observational datasets is most realistic. For example, since the CERES EBAF surface radiative fluxes are a derived product (being parameterized based on the measured TOA fluxes), they are not necessarily more reliable than the surface radiative fluxes in the two reanalyses. We conclude, therefore, that large discrepancies in Antarctic surface energy fluxes between existing observational products preclude any meaningful evaluation of CMIP5 biases in these fluxes.

### b. Causes of excessive TOA SW absorption during summer

We now return our attention to the CMIP5 biases in the TOA SW flux during austral summer (DJF). The multimodel mean bias in this flux is  $+9.8 \pm 1.1 \text{ W m}^{-2}$ , where the uncertainty range is the  $2\sigma$  intraensemble spread of the TOA SW biases (averaged over all models with multiple ensemble members). That this uncertainty is small relative to the multimodel mean bias suggests that the latter is not a sampling artifact resulting from the comparison of a single 10-yr period in observations

with the CMIP5 multimodel mean climatology. In other words, we can conclude that the difference between the simulated and observed TOA SW flux cannot be explained by internal climate variability.

To better understand the causes of the models' excessive TOA SW absorption, we decompose the multimodel mean bias as follows:

$$\begin{aligned} \text{BIAS}_{\text{TOA\_SW}} &= \text{BIAS}_{\text{SW}\downarrow} - \text{BIAS}_{\text{SW}\uparrow(\text{clr})} + \text{BIAS}_{\text{SW\_CRE}} \\ &= \text{BIAS}_{\text{SW}\downarrow} - \text{BIAS}_{\text{SW}\uparrow(\text{clr})} \\ &\quad + [\text{BIAS}_{\text{SW}\uparrow(\text{clr})} - \text{BIAS}_{\text{SW}\uparrow}]. \end{aligned} \quad (6)$$

Equation (6) states that the total bias in the TOA net incoming SW radiation ( $\text{BIAS}_{\text{TOA\_SW}}$ ) comprises the biases in three separate components: the downward SW flux at the TOA ( $\text{BIAS}_{\text{SW}\downarrow}$ ), the upward SW flux at the TOA under clear skies [ $\text{BIAS}_{\text{SW}\uparrow(\text{clr})}$ ], and the SW cloud-radiative effect ( $\text{BIAS}_{\text{SW\_CRE}}$ ). The clear-sky upward SW flux at the TOA represents the reflection of solar radiation by the surface, atmospheric gases, and aerosols. The SW cloud-radiative effect (CRE; also commonly referred to as the cloud-radiative forcing) quantifies the additional solar reflection due to the presence of clouds.

For the CMIP5 multimodel mean, we find that  $\text{BIAS}_{\text{SW}\downarrow} = +3.1 \text{ W m}^{-2}$ ,  $\text{BIAS}_{\text{SW}\uparrow(\text{clr})} = -5.0 \text{ W m}^{-2}$ , and  $\text{BIAS}_{\text{SW\_CRE}} = +1.7 \text{ W m}^{-2}$  (all relative to CERES EBAF TOA data). Thus, all three terms on the right-hand side of Eq. (6) contribute to the positive bias in the TOA net SW flux. The largest contributor is a negative bias of  $-5.0 \text{ W m}^{-2}$  in the clear-sky SW reflection. In accordance with this, we find that the multimodel mean surface albedo, averaged over the  $70^\circ$ – $90^\circ\text{S}$  region, is lower than the corresponding value based on CERES data (0.72 and 0.74, respectively). While a mere 2% difference in albedo may seem trivial, it must be borne in mind that the clear-sky surface downwelling SW radiation is very large over the Antarctic during austral summer, being about  $360 \text{ W m}^{-2}$  in the multimodel mean. Therefore, even such a modest albedo difference would serve to increase the surface absorption of SW radiation by  $7.2 \text{ W m}^{-2}$  in the models, which is more than enough to account for the bias in the clear-sky reflection.

After  $\text{BIAS}_{\text{SW}\uparrow(\text{clr})}$ , the next most important term is  $\text{BIAS}_{\text{SW}\downarrow}$ . The latter indicates that the CMIP5 models have too much solar energy input at the TOA, a bias that has been noted previously (e.g., Schmidt et al. 2014) in model simulations of the first decade of the current century. This error is related to the inadequate representation in the models of the recent deep and

prolonged solar cycle minimum. Finally, a positive bias of  $+1.7 \text{ W m}^{-2}$  in the SW CRE also contributes to the bias in the TOA net SW flux. The SW CRE is defined as the difference in the upward (reflected) SW flux at the TOA between clear-sky and all-sky conditions [see Eq. (6)]. This difference is almost always negative since clouds (i.e., all-sky conditions) generally enhance the reflection of solar radiation compared to what occurs under clear skies. Thus, the positive CMIP5 bias in the SW CRE signifies that this additional solar reflection due to the presence of clouds is not as large in the models as observed. This indicates either that there are too few clouds in the models and/or that the simulated clouds are not as bright as they should be (see also Trenberth and Fasullo 2010).

Apart from exhibiting a significant multimodel mean bias, there is also a considerable amount of intermodel spread in the simulated TOA SW flux during DJF (see Fig. 3a). We find that nearly all of this intermodel spread can be accounted for by differences in surface albedo between the models, as illustrated in Fig. 4. Albedo differences explain 92% of the variance in the simulated TOA SW flux. Similarly, these differences also explain almost all (93%) of the variance in the DJF surface SW flux (not shown). The variability in surface albedo across the CMIP5 models is related in part to differences in the total sea ice–covered area within the  $70^{\circ}$ – $90^{\circ}$ S domain. In this region, simulated total SIE is significantly correlated with the area-averaged surface albedo during the DJF season ( $r = 0.45$ , significant at the 95% level). Even though there clearly must be other factors contributing to the intermodel spread in surface albedo (e.g., differences in the albedo of the Antarctic continent), this correlation nevertheless implies a relationship between SIE and the DJF SW radiation at both the TOA and surface. In the next section, we quantify the strength of this relationship and further assess the impact of sea ice on other components of the Antarctic energy budget.

### c. Importance of sea ice

Figure 5 shows correlations across the CMIP5 models between the total SIE (over  $70^{\circ}$ – $90^{\circ}$ S) and the individual terms in the Antarctic energy budget. For the DJF net downward SW fluxes discussed above, the correlation is negative and positive at the TOA and surface, respectively. This opposite-signed correlation occurs because the net downward SW flux is defined to be positive at the TOA but negative at the surface (see section 2a). Thus, this net flux decreases (increases) at the TOA (surface) as SIE increases as a result of the associated enhanced reflection of SW radiation. At both levels in the atmosphere, there is a similar correlation between SIE and the net SW flux during other seasons of the year

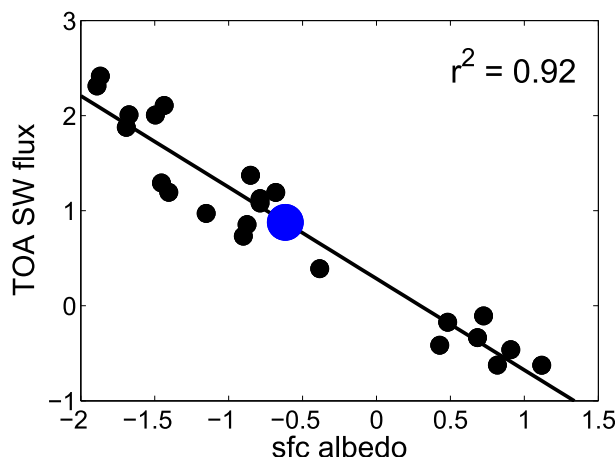


FIG. 4. CMIP5 standardized biases in the TOA net shortwave (SW) radiation vs surface albedo during DJF. Albedo biases are relative to the CERES EBAF surface dataset. Black dots represent individual CMIP5 models, and the larger blue dot represents the multimodel mean. The black line depicts the least squares linear fit to the data.

and in the annual mean. The notable exception to this is a relatively weak correlation (at both the TOA and surface) during the June–August (JJA) season, when insolation is minimal over the Southern Hemisphere polar cap. The correlation between SIE and the DJF surface SW flux is statistically significant at the 95% confidence level (dashed black lines in Fig. 5). Correlations that are significant at the 90% level occur for the surface SW flux in MAM, September–November (SON), and the annual mean and for the TOA SW flux in DJF and SON.

In terms of LW radiation, there is a statistically significant positive correlation at the TOA during MAM that appears as a similar correlation with the TOA net radiation. Since the outgoing longwave radiation (OLR) at the TOA is defined to be negative in the present study, this positive correlation implies reduced OLR as SIE increases. This OLR decrease is partly due to lower temperatures over the Antarctic region, with the polar-cap-averaged surface air temperature found to be inversely correlated with total SIE during MAM ( $r = -0.52$ , significant at the 95% level).

Additional significant (inverse) correlations are indicated in Fig. 5 between SIE and the surface LH + SH flux in MAM, JJA, and the annual mean. These correlations lead to similar correlations between SIE and the surface net energy flux (with the latter actually being somewhat stronger). Examining the LH and SH fluxes separately, we find that the former dominate the correlations between SIE and the total turbulent energy flux. In MAM, JJA, and the annual mean, the correlations between SIE and the surface LH flux are  $-0.86$ ,  $-0.71$ ,

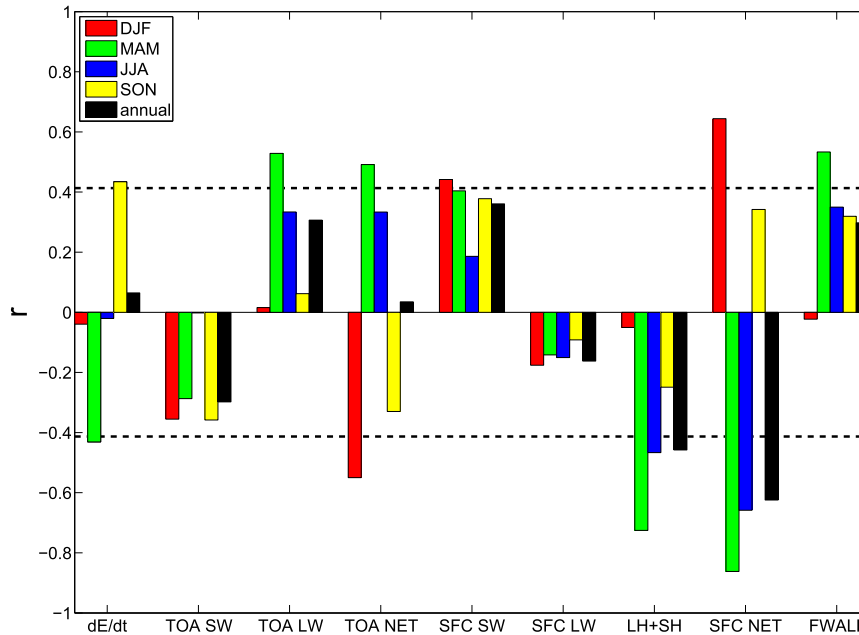


FIG. 5. Correlations between the climatological mean energy budget terms and total SIE over 70°–90°S. For each energy budget term, different colors represent different seasons and the annual mean (see the legend). Dashed black lines indicate the 95% significance level.

and  $-0.75$ , respectively. The corresponding values in MAM, JJA, and the annual mean for the surface SH flux are  $-0.54$ ,  $-0.25$  and  $-0.17$ , with only the MAM correlation being statistically significant. For both the LH and SH fluxes, these negative correlations signify an anomalous downward turbulent energy transfer at the surface as SIE increases. This is consistent with greater ice cover more effectively shielding the Antarctic atmosphere from oceanic sources of heat and moisture.

Finally, it is important to point out that the relationships between sea ice and the Antarctic energy budget discussed in this section may work in both directions. In other words, just as differences in sea ice across the CMIP5 models may explain differences in the energy fluxes, the latter, in turn, may drive intermodel differences in sea ice. Consider, for example, the significant correlation between SIE and the surface SW radiation during austral summer (see Fig. 5). One could hypothesize that differences in oceanic forcing (e.g., in the upwelling of relatively warm water) between models might trigger some initial difference in SIE. Models with less sea ice would then absorb more SW radiation at the ocean surface, contributing to ice melt and thereby reinforcing the initial SIE difference. (This is, in fact, the essence of the sea ice–albedo feedback.) Our intent here is simply to document the existence of these relationships in the CMIP5 models between the simulated SIE and Antarctic energy budget, with the understanding

that causality in these relationships is likely to work in both directions to some degree.

#### 4. Summary and conclusions

In this paper, we have evaluated how well the current generation of global climate models, the CMIP5 coupled atmosphere–ocean GCMs, simulate the observed present-day (2001–10) Antarctic atmospheric energy budget. This represents a fundamental test of model performance and adds to the growing body of recent work assessing GCM skill in the Southern Hemisphere.

We find that the CMIP5 models simulate the gross features of the climatological mean Antarctic energy budget remarkably well. The models correctly capture the approximate two-way balance between the TOA net radiative energy loss and the energy gain through atmospheric transport into the polar cap. Observed seasonal cycles in these two terms, as well as the atmospheric energy storage, are realistically simulated (Fig. 2).

Despite this overall agreement between models and observations, the simulated TOA net incoming SW radiation during austral summer was found to be too large by approximately  $10 \text{ W m}^{-2}$  in the multimodel mean (and by as much as  $25\text{--}30 \text{ W m}^{-2}$  in individual models; see Fig. 3a). This excess in absorbed solar radiation over the Antarctic is also a characteristic bias of current

climate models at Southern Hemisphere midlatitudes (Trenberth and Fasullo 2010; Ceppi et al. 2012; Hwang and Frierson 2013; Li and Xie 2014). At midlatitudes, the bias has been attributed principally to errors in the simulated cloud field (Trenberth and Fasullo 2010). This is not the case over the Antarctic, however. While model cloud errors contribute here as well to the excess in absorbed solar radiation, they are secondary in importance compared to errors in the simulated clear-sky SW reflection (related to surface albedo errors) and in the downwelling SW at the TOA (related to the recent deep and prolonged solar minimum).

At the Antarctic surface, there are substantial differences in the climatological energy fluxes between three observational products that we examined: ERA-Interim, the NCEP–NCAR reanalysis, and the CERES EBAF surface dataset. In individual seasons, these differences can exceed  $40 \text{ W m}^{-2}$  (see Fig. 3b). It is not immediately clear which observational product(s) is the most reliable. For example, although attempts have been made to validate the reanalysis-based surface energy budget in the Antarctic (e.g., Hines et al. 1999), these validation efforts have by necessity (i.e., because of sparse in situ measurements) been limited to individual seasons and subregions of the Antarctic. In other words, to our knowledge, there exist no published estimates of the errors in reanalysis-based representations of the surface energy budget in a climatological mean and Antarctic-wide sense. Given this, as well as the large differences between observational products noted above, we are prevented from drawing any conclusions about the accuracy of the simulated surface energy fluxes in the CMIP5 models.

Finally, the present study has highlighted the strong relationships that exist between the model-simulated sea ice and Antarctic energy budget (see Fig. 5). For instance, through its impact on the surface albedo, sea ice extent (SIE) is closely linked with the amount of absorbed solar radiation at both the TOA and surface. Additionally, by serving as a buffer between the atmosphere and underlying ocean, sea ice strongly modulates the surface turbulent energy exchange. Since the CMIP5 models are known to exhibit biases in their simulation of Antarctic SIE (Turner et al. 2013), one might then expect that these biases would translate into biases in the simulated energy fluxes. In accordance with this, our results suggest that the models' tendency to underestimate the observed annual minimum in SIE (Turner et al. 2013) contributes to the simulated negative bias in the clear-sky reflection of SW radiation at the TOA. As discussed in section 3b, this negative bias in the clear-sky reflection is the primary contributor to the excessive TOA SW absorption that is simulated during summer. We conclude, therefore, that

reducing Antarctic sea ice biases in current climate models should be set as a top priority for future work. Doing so will allow for a more realistic simulation of the flows of energy through the Antarctic atmosphere and their future changes in response to anthropogenic forcing.

*Acknowledgments.* We thank three anonymous reviewers whose comments significantly improved the manuscript. We gratefully acknowledge support from the NSF Division of Polar Programs, PLR 13-41657. We also acknowledge the World Climate Research Programme's Working Group on Coupled Modelling, which is responsible for CMIP, and we thank the climate modeling groups for producing and making available their model output.

## REFERENCES

- Barnes, E. A., and D. L. Hartmann, 2010: Testing a theory for the effect of latitude on the persistence of eddy-driven jets using CMIP3 simulations. *Geophys. Res. Lett.*, **37**, L15801, doi:10.1029/2010GL044144.
- Bintanja, R., G. J. van Oldenborgh, S. S. Drijfhout, B. Wouters, and C. A. Katsman, 2013: Important role for ocean warming and increased ice-shelf melt in Antarctic sea-ice expansion. *Nat. Geosci.*, **6**, 376–379, doi:10.1038/ngeo1767.
- Bracegirdle, T. J., E. Shuckburgh, J. B. Sallee, Z. Wang, A. J. S. Meijers, N. Bruneau, T. Phillips, and L. J. Wilcox, 2013: Assessment of surface winds over the Atlantic, Indian, and Pacific Ocean sectors of the Southern Ocean in CMIP5 models: Historical bias, forcing response, and state dependence. *J. Geophys. Res. Atmos.*, **118**, 547–562, doi:10.1002/jgrd.50153.
- Ceppi, P., Y. T. Hwang, D. M. W. Frierson, and D. L. Hartmann, 2012: Southern Hemisphere jet latitude biases in CMIP5 models linked to shortwave cloud forcing. *Geophys. Res. Lett.*, **39**, L19708, doi:10.1029/2012GL053115.
- Chang, E. K. M., Y. Guo, and X. Xia, 2012: CMIP5 multimodel ensemble projection of storm track change under global warming. *J. Geophys. Res.*, **117**, D23118, doi:10.1029/2012JD018578.
- , —, —, and M. Zheng, 2013: Storm-track activity in IPCC AR4/CMIP3 model simulations. *J. Climate*, **26**, 246–260, doi:10.1175/JCLI-D-11-00707.1.
- Dee, D. P., and Coauthors, 2011: The ERA-Interim reanalysis: Configuration and performance of the data assimilation system. *Quart. J. Roy. Meteor. Soc.*, **137**, 553–597, doi:10.1002/qj.828.
- Fan, T., C. Deser, and D. P. Schneider, 2014: Recent Antarctic sea ice trends in the context of Southern Ocean surface climate variations since 1950. *Geophys. Res. Lett.*, **41**, 2419–2426, doi:10.1002/2014GL059239.
- Gagné, M.-È., N. P. Gillett, and J. C. Fyfe, 2015: Observed and simulated changes in Antarctic sea ice extent over the past 50 years. *Geophys. Res. Lett.*, **42**, 90–95, doi:10.1002/2014GL062231.
- Grise, K. M., and L. M. Polvani, 2014: Southern Hemisphere cloud-dynamics biases in CMIP5 models and their implications for climate projections. *J. Climate*, **27**, 6074–6092, doi:10.1175/JCLI-D-14-00113.1.
- Heuzé, C., K. J. Heywood, D. P. Stevens, and J. K. Ridley, 2013: Southern Ocean bottom water characteristics in CMIP5 models. *Geophys. Res. Lett.*, **40**, 1409–1414, doi:10.1002/grl.50287.
- Hines, K. M., R. W. Grumbine, D. H. Bromwich, and R. I. Cullather, 1999: Surface energy balance of the NCEP

- MRF and NCEP–NCAR reanalysis in Antarctic latitudes during FROST. *Wea. Forecasting*, **14**, 851–866, doi:10.1175/1520-0434(1999)014<0851:SEBOTN>2.0.CO;2.
- Hosking, J. S., A. Orr, G. J. Marshall, J. Turner, and T. Phillips, 2013: The influence of the Amundsen–Bellingshausen Seas low on the climate of West Antarctica and its representation in coupled climate model simulations. *J. Climate*, **26**, 6633–6648, doi:10.1175/JCLI-D-12-00813.1.
- Hwang, Y. T., and D. M. W. Frierson, 2013: Link between the double-Intertropical Convergence Zone problem and cloud biases over the Southern Ocean. *Proc. Natl. Acad. Sci. USA*, **110**, 4935–4940, doi:10.1073/pnas.1213302110.
- Kalnay, E., and Coauthors, 1996: The NCEP/NCAR 40-Year Reanalysis Project. *Bull. Amer. Meteor. Soc.*, **77**, 437–471, doi:10.1175/1520-0477(1996)077<0437:TNYRP>2.0.CO;2.
- Kato, S., N. G. Loeb, F. G. Rose, D. R. Doelling, D. A. Rutan, T. E. Caldwell, L. Yu, and R. A. Weller, 2013: Surface irradiances consistent with CERES-derived top-of-atmosphere shortwave and longwave irradiances. *J. Climate*, **26**, 2719–2740, doi:10.1175/JCLI-D-12-00436.1.
- Kidston, J., and E. P. Gerber, 2010: Intermodel variability of the poleward shift of the austral jet stream in the CMIP3 integrations linked to biases in 20th century climatology. *Geophys. Res. Lett.*, **37**, L09708, doi:10.1029/2010GL042873.
- Li, G., and S. P. Xie, 2014: Tropical biases in CMIP5 multimodel ensemble: The excessive equatorial Pacific cold tongue and double ITCZ problems. *J. Climate*, **27**, 1765–1780, doi:10.1175/JCLI-D-13-00337.1.
- Loeb, N. G., B. A. Wielicki, D. R. Doelling, G. L. Smith, D. F. Keyes, S. Kato, N. Manalo-Smith, and T. Wong, 2009: Toward optimal closure of the earth's top-of-atmosphere radiation budget. *J. Climate*, **22**, 748–766, doi:10.1175/2008JCLI2637.1.
- Polvani, L. M., and K. L. Smith, 2013: Can natural variability explain observed Antarctic sea ice trends? New modeling evidence from CMIP5. *Geophys. Res. Lett.*, **40**, 3195–3199, doi:10.1002/grl.50578.
- Previdi, M., K. L. Smith, and L. M. Polvani, 2013: The Antarctic atmospheric energy budget. Part I: Climatology and intraseasonal-to-interannual variability. *J. Climate*, **26**, 6406–6418, doi:10.1175/JCLI-D-12-00640.1.
- Schmidt, G. A., D. T. Shindell, and K. Tsigaridis, 2014: Reconciling warming trends. *Nat. Geosci.*, **7**, 158–160, doi:10.1038/ngeo2105.
- Smith, K. L., M. Previdi, and L. M. Polvani, 2013: The Antarctic atmospheric energy budget. Part II: The effect of ozone depletion and its projected recovery. *J. Climate*, **26**, 9729–9744, doi:10.1175/JCLI-D-13-00173.1.
- Trenberth, K. E., 1991: Climate diagnostics from global analyses: Conservation of mass in ECMWF analyses. *J. Climate*, **4**, 707–722, doi:10.1175/1520-0442(1991)004<0707:CDFGAC>2.0.CO;2.
- , and J. T. Fasullo, 2010: Simulation of present-day and twenty-first-century energy budgets of the southern oceans. *J. Climate*, **23**, 440–454, doi:10.1175/2009JCLI3152.1.
- Turner, J., T. J. Bracegirdle, T. Phillips, G. J. Marshall, and J. S. Hosking, 2013: An initial assessment of Antarctic sea ice extent in the CMIP5 models. *J. Climate*, **26**, 1473–1484, doi:10.1175/JCLI-D-12-00068.1.